BULLETIN OF THE POLISH ACADEMY OF SCIENCES
TECHNICAL SCIENCES
Vol. 53, No. 4, 2005

Numerical simulation of multiple species detection using hydrodynamic/electrokinetic focusing

J. HAHM and A. BESKOK*

Mechanical Engineering Department, Texas A&M University, Bio-Micro-Fluidics Laboratory, College Station TX 77843–3123, USA

Abstract. In this paper we present the numerical simulation-based design of a new microfluidic device concept for electrophoretic mobility and (relative) concentration measurements of dilute mixtures. The device enables stationary focusing points for each species, where the locally applied pressure driven flow (PDF) counter balances the species' electrokinetic velocity. The axial location of the focusing point, along with the PDF flowrate and applied electric field reveals the electrokinetic mobility of each species. Simultaneous measurement of the electroosmotic mobility of an electrically neutral specie can be utilized to calculate the electrophoretic mobility of charged species. The proposed device utilizes constant sample feeding, and results in time-steady measurements. Hence, the results are independent of the initial sample distribution and flow dynamics. In addition, the results are insensitive to the species diffusion for large Peclet number flows ($Pe > 400$), enabling relative concentration measurement of each specie in the dilute mixture.

Key words: Species detection, electrophoresis, hydrodynamic/electrokinetic focusing, microfluidics.

1. Introduction

Electroosmosis and electrophoresis are the leading electrokinetic effects utilized in microfluidic systems. Electroosmosis is the motion of an ionized fluid relative to the stationary charged surface by an applied electric field [1]. It enables fluid pumping and flow control in microchannels using electric fields, eliminating the need for mechanical pumps with moving components. Electrophoresis is the motion of charged particles and macromolecules relative to a stationary liquid by an applied electric field [2]. Both of these electrokinetic effects are utilized in the design of micro-total-analysis systems (μ-TAS) for biomedical, pharmaceutical and environmental monitoring applications. Particularly, electrophoresis is one of the most extensively utilized techniques for separation and/or characterization of charged particles, and biological molecules [3–5]. For example, proteins, amino acids, peptides, nucleotides and polynucleotides can be separated using electrophoretic techniques. Such electric charge-based separation techniques are being utilized for species detection/identification in μ-TAS.

Among the several electrophoresis processes, steady state and capillary zone electrophoresis are the two mostly utilized techniques in microfluidic applications. The steady state electrophoresis is obtained, when the spatial location of separated components do not change in time. It is commonly observed in isoelectric focusing (IEF), where charged particles migrate under electrophoretic forcing and pH gradients to a location in the buffer, where they experience zero net charge. This location is known as the isoelectric point. Overall, the IEF is used to separate, as well as concentrate charged species under pH gradients [6–10]. The capillary zone electrophoresis utilizes a supporting medium to hold the sample, while an external electric potential is applied at the end of the supporting media. Typically, a buffer solution, filter paper, cellulose, cellulose-acetate or gel are used as the supporting media [11,12]. The capillary electrophoresis has utmost potential for development of automated analytical equipment with fast analysis time and on-line detection possibilities. Currently, many separation techniques rely on combined capillary electrophoresis and electroosmotic flow to pump solutes towards the detector [13].

In this paper we present numerical modeling results of a new species detection concept, which exhibits discrete stationary focusing points for multiple species, based on their electric charge. Although the device utilizes processes similar to the capillary electrophoresis, it uses a balance between the electrokinetic mobility of the species and the PDF to result in stationary focusing points, similar to the isoelectric focusing. In the next section we discuss the governing equations and our numerical simulation methodology, which is followed by description of the mobility measurement device with specific numerical examples and theoretical analyses based on one-dimensional conservation laws. Finally, we conclude by summarizing the advantages and limitations of the proposed device concept, and make comparisons with other charge-based species separation and detection techniques.

2. Governing equations and numerical formulation

In this paper, we summarize the governing equations for electrokinetic flows. Detailed discussions on the electrokinetic transport can be found in [1,13]. The electrokinetic phenomena are present due to the electric double layer (EDL), which forms as a result of the interaction of ionized solution with static charges on dielectric surfaces. For example, when silica is in contact with an aqueous solution, its surface hydrolyzes

*e-mail: abeskok@tamu.edu

to form silanol surface groups. These groups may be positively charged as $Si-OH_2^+$, neutral as $Si-OH$, or negatively charged as $Si-O^-$, depending on the pH value of the electrolyte solution. If the channel surface is negatively charged (such as in the case of deionized water), the positive ions are attracted towards the surface, and the negative ions are repelled from the surface, keeping bulk of the liquid, far away from the wall, electrically neutral. Depending on the ionic concentration, the EDL thickness varies from 3 nm to 300 nm. For a symmetric electrolyte with equal valance, ion redistribution within the EDL can be modeled using the Poisson-Boltzmann equation, which utilizes an electrokinetic potential. The electrokinetic potential decays to zero outside the EDL region, and it reaches a finite value on the surface that is known as the Zeta potential (ζ). Typical physical and electrochemical conditions observed in electrokinetic micro-flows are presented in Tab. 1.

Table 1
Typical physical and electrochemical parameters utilized in micro–scale electrokinetic flows

Parameter	Parameter range
Typical channel half thickness, h (μm)	$0.1 \sim 100$
Electrolyte concentration, n_o (mM)	$100 \sim 0.01$
Debye length, λ (nm)	$1 \sim 100$
Zeta potential, ζ (mV)	$\pm 25 \sim \pm 100$
Electric field, $\vec{E}$ (V/mm)	$1 \sim 100$
Reynolds number, Re	$10^{-4} \sim 1$

For electrokinetic transport, we solve the incompressible Navier–Stokes equations given by

$$\rho\left(\frac{\partial \vec{u}}{\partial t} + (\vec{u}\cdot\nabla)\vec{u}\right) = -\nabla p + \eta\nabla^2\vec{u}, \tag{1}$$

where p is the pressure, ρ is the fluid density, η is the absolute viscosity, and $\vec{u}$ is the velocity vector that satisfies the incompressibility condition ($\nabla\cdot\vec{u}=0$). In this approximation, we ignore the velocity distribution within the thin EDL region, and model electrokinetic effects using the Helmholtz-Smoluchowski slip velocity (u_{HS}), given by [13]

$$\vec{u}_{HS} = \frac{-\zeta\epsilon}{\eta}\vec{E}, \tag{2}$$

where ϵ, is the electric permittivity of the buffer. The externally applied electric field, $\vec{E}$, is modelled as

$$\vec{E} = -\nabla\phi, \tag{3}$$

where ϕ is the electrostatic potential, which obeys the Laplace's equation. We specify ϕ on electrode surfaces, while no-penetration conditions are specified on the dielectric surfaces. Due to the zero flux conditions, Eq. (2) gives slip velocities tangent to the dielectric surface. Although the Helmholtz-Smoluchowski slip velocity ignores the velocity distribution within the EDL region, it accurately models electrokinetically induced flows in the bulk flow region, even for transient and time-periodic flows [14]. Utilization of the Helmholtz-Smoluchowski slip velocity reduces the numerical stiffness induced by the need to accurately resolve the thin EDL region of the flow, which is orders of magnitudes smaller than the characteristic channel height.

The alternative modeling approach is to resolve the flow in the entire domain, including the EDL region. Since the fluid in the EDL is electrically charged, solution of the Poisson-Boltzmann equation results in an electric charge density (ρ_e). This induces an electrokinetic body force ($\rho_e\vec{E}$) on the flow, strictly active within the EDL region, when subjected to an externally applied electric field ($\vec{E}$). This modeling approach requires proper resolution of the flow and electrokinetic potential within the EDL. First, by solving the Poisson-Boltzmann equation to obtain the electric charge density, and then solving the Navier–Stokes Eqs (1) augmented by this body force ($\rho_e\vec{E}$), subjected to the no-slip boundary condition on the walls.

In absence of chemical reactions, the charged species conservation equation for multi-component fluid is given as

$$\frac{\partial c_i}{\partial t} + \nabla\vec{j}_i = 0, \tag{4}$$

where c_i is the concentration of the i^{th} species and $\vec{j}_i$ is the species flux given by

$$\vec{j}_i = -D_i\nabla c_i + c_i\left[\vec{u} + \mu_{ep,i}\vec{E}\right], \tag{5}$$

where D_i is the diffusion coefficient, and $\mu_{ep,i}$ is the electrophoretic mobility. The first term on the right hand side shows molecular diffusion flux due to the concentration gradient, while the second term shows convection due to bulk fluid motion with velocity $\vec{u}$, which includes both hydrodynamic and electroosmotic transport effects. The last term represents electrophoretic transport due to the electrophoretic mobility, which is related to the electrophoretic migration velocity $\vec{u}_{ep}$ by

$$\vec{u}_{ep} = \mu_{ep}\vec{E}. \tag{6}$$

The Navier-Stokes and species transport equations are solved after proper normalization. We have chosen a characteristic channel dimension h, and the Helmholtz-Smoluchowski velocity U_{HS} to normalize the length and velocity scales in the problem, respectively. Species concentration is normalized using a reference species concentration value c_o. All non–dimensional parameters are shown using superscript *. For example, $x^* = x/h$, $u^* = u/U_{HS}$, $v^* = v/U_{HS}$, $t^* = tU_{HS}/h$, and $c^* = c/c_o$. Proper normalization of the governing equations result in the Reynolds (Re) and Peclet (Pe) numbers as the two important non–dimensional parameters for this problem. The Reynolds number is defined as

$$Re = \frac{hU_{HS}}{\nu},$$

where ν is the kinematic viscosity. The Peclet number is defined as

$$Pe = \frac{hU_{HS}}{D},$$

where D is the species diffusion coefficient. In this definition, the Pe is based on the Schmidt number ($Sc = \nu/D$), and hence $Pe = Re \times Sc$. Due to the small length scales, micro–flows often experience Stokes flow ($Re < 1$) conditions. However, the diffusion coefficients for large particles suspended in aqueous solutions are often very small, as can be predicted using the Stokes-Einstein relation [13]. Therefore,

the Schmidt numbers for large particles, such as flow-tracing dyes and bio–molecules, are often in the range of $Sc = 1 \times 10^5$ [15]. This creates a rather unique transport phenomena: In micro-flows, the momentum transport is dominated by viscous forces ($Re < 1$), while the species transport is convection dominated ($Pe \simeq 1000$). Although this unique feature makes mixing in micro–scales rather challenging, convection dominated flow is important for our device concept.

Details of our numerical algorithm was presented in a previous paper [16]. The algorithm is based on the spectral element method (SEM), which discretizes the computational domain into quadrilateral elements, similar to the (low-order) finite element method (FEM). However, each element is further discretized using a specific set of Jacobi polynomials. This choice enables us to enrich the elemental discretization simply by increasing the order of the interpolation polynomials. Increasing the order of each element by keeping the number of elements unchanged is known as p-type refinement. Increasing the number of elements while keeping the elemental expansion order the same is known as h-type refinement. Although both refinement techniques result in increased accuracy, the p-type refinement leads to exponential reduction of discretization errors (spectral convergence) due to the approximation properties of the Jacobi polynomials, while the h-type refinement results in algebraic convergence [17]. Spectral convergence is an important advantage of the SEM, since it is possible to reduce the discretization errors by at least two orders of magnitudes, by simply doubling the degrees of freedom per direction. Our flow solver utilizes the operator splitting scheme, and results in third-order time and spectral spatial accuracy [18]. Further details of our numerical formulation, and code verification can be found in [16,19]. Code validation with experimental data was presented in [20]. All results presented in the following section were tested for grid independence by successive p-type refinements, and monitoring the global error in the conservation of momentum equation, which was well below 0.1%.

3. Mobility measurement device

The basic design, shown in Fig. 1, consists of multiple parallel channels that gradually expand to the main channel downstream of the device. We have chosen the inner channel half height h_o as the characteristic dimension, and described other length scales in terms of h_o. The device width (W) is in to the page direction, and not shown in the figure. In this schematics and the following numerical simulations, we have utilized 5 progressively expanding channels with half height of h_i, $(i = 1, ..., 5)$. Each progressive channel is ΔL longer than the previous one ($L_i = L_{i-1} + \Delta L$), and the main channel length is L_5. In the following, we will ignore the individual channel thickness, and their effects on the flow and electric field for simplicity. We will present one-dimensional theoretical analysis and two-dimensional numerical solutions of hydrodynamic and electrokinetic transport in the device.

3.1. Hydrodynamic flow. All channels on left side of the device, shown in Fig. 1 are closed, with the exception of the inner channel that is connected to a syringe pump, where a pressure driven flow with a prescribed flowrate of $\dot{Q}$ is imposed from left to right. The channel width W (into the page direction in Fig. 1) is assumed much larger than the maximum channel height h_5, so that we approximate the flow as two–dimensional by neglecting the blockage effects from the top and bottom surfaces of the device. Therefore, the volumetric flowrate per channel width is

$$\dot{q} = \frac{\dot{Q}}{W}, \tag{7}$$

while the channel averaged hydrodynamic velocity ($\bar{u}_i$) in each channel becomes

$$\bar{u_i} = \frac{\dot{q}}{h_i}. \tag{8}$$

Using this one-dimensional analysis, we observe that channel averaged velocity in the device is progressively reduced by increasing h_i. One can design a similar device using tens of progressively expanding channels. At the same time, it is possible to regulate the channel averaged velocity in each channel using the channel height ratio, since

$$\bar{u_i} h_i = \bar{u_o} h_o = \dot{q}. \tag{9}$$

In the following, we decided to obtain $\bar{u_i} = (1.0 - 0.1 \times i) \times \bar{u_0}$ in each channel. Hence, we utilized $h_o = (1.0 - 0.1 \times i) \times h_i$. For example, this reduces the channel averaged velocity to $0.5 \times \bar{u_o}$ in the 5^{th} (main) channel by using $h_5 = 2 \times h_o$.

In order to investigate the effects of two–dimensional viscous flow, we numerically solved the Navier–Stokes equations in the device using channel expansion geometry described by $h_o = (1.0 - 0.1 \times i) \times h_i$. The stream–wise and span–wise velocity contours for Reynolds (Re) number 0.01 flow are shown in Fig. 2 for two separate configurations, utilizing $\Delta L = 10 h_o$ (left) and $\Delta L = 4 h_o$ (right). The bottom row of Fig. 2 shows the normalized streamwise velocity (u^*) variation at the centerline of the device (see also Fig. 1). We observe that the $\Delta L = 10 h_o$ case results in step–like reduction in the centerline velocity, where u^* remains fairly constant between the channel expansion regions. This basically results in fully developed Poiseuille flow in between the channel expansion regions due to the small Re flow. On the other hand, the $\Delta L = 4 h_o$ geometry results in velocity contours similar to the gradually expanding flow in a diffuser. This case results in (almost) linear decrease in the centerline velocity u^* with increased streamwise distance x^*. These two cases demonstrate two separate characteristics for the proposed device. The $\Delta L = 10 h_o$ and $\Delta L = 4 h_o$ cases lead to the "digitized" and "analog" versions of the device concept, respectively.

3.2. Electric field and electrokinetic flow. The design includes electrodes located on the right and left sides of the device (Fig. 1), where we apply an axial electric field in the channel. Ignoring the channel thickness effects, the device experiences uniform electric field. Under these conditions, the electrokinetic transport can be simply modeled using the electrokinetic mobility μ_{ek} concept. For a given uniform electric field E, each specie i will experience a different electrokinetic velocity $u_{ek,i}$

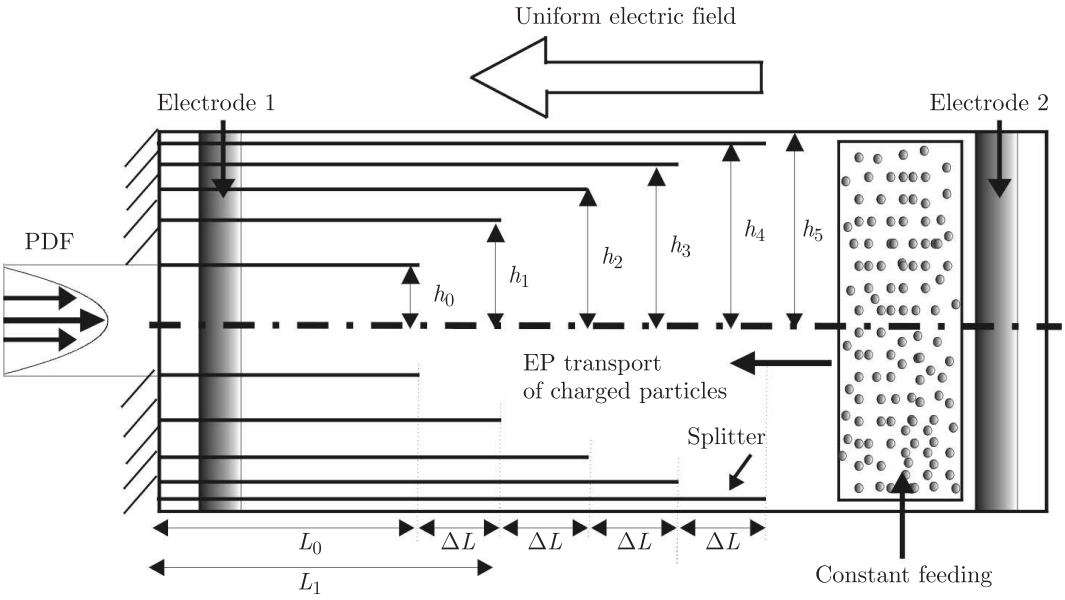

Fig. 1. Schematic view of the proposed device concept

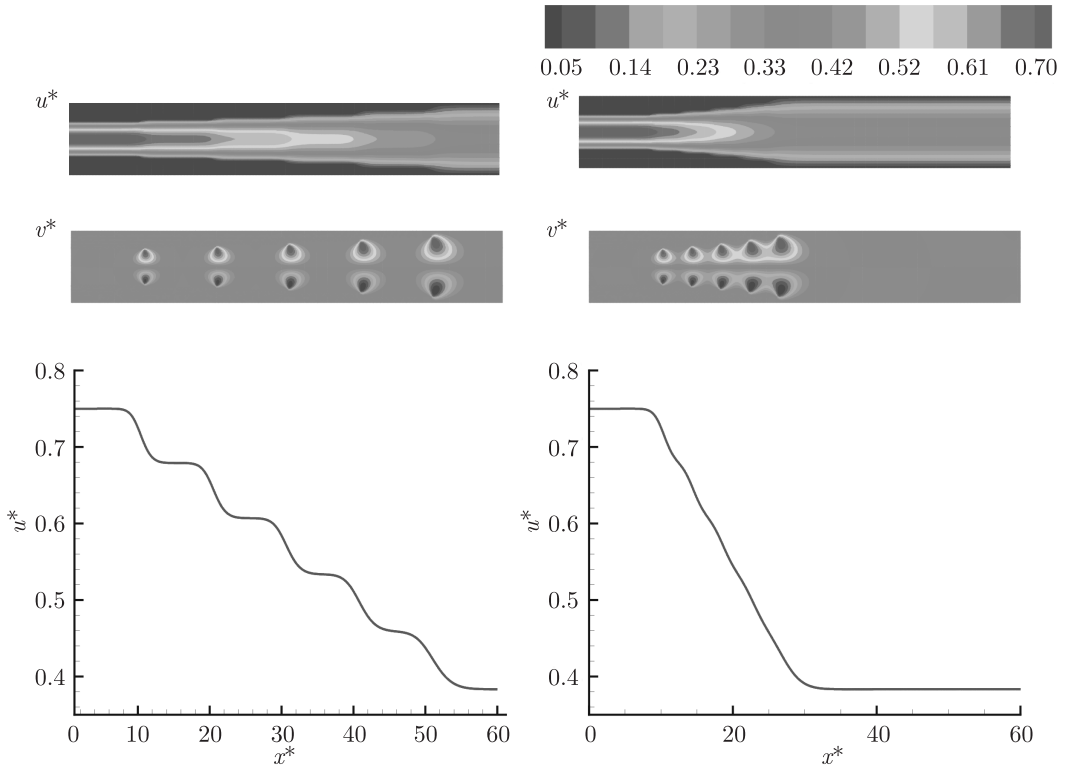

Fig. 2. Pressure driven flow velocity contours (u^*– stream wise; v^*– span wise) and velocity distribution at the channel centerline for $\Delta L = 10h_o$ (left column) case and $\Delta L = 4h_o$ (right column) case

$$u_{ek,i} = \mu_{ek,i} E. \tag{10}$$

Due to the uniform axial electric field, the electrokinetic velocity of each specie is in the axial direction, and $u_{ek,i}$ is a constant in the entire device. Electrokinetic mobility of charged species can be written as a superposition of the species electrophoretic mobility (μ_{ep}), and the electroosmotic mobility (μ_{eo}) of the buffer solution:

$$\mu_{ek} = \mu_{ep} + \mu_{eo}. \tag{11}$$

The electroosmotic flow (EOF) is generated when an axial electric field is imposed in presence of an ionized fluid that is in contact with a dielectric surface [1]. Therefore, the electrically

neutral buffer experiences electroosmotic motion. Depending on the polarity of ion distribution within the electrical double layer, the EOF will be towards the oppositely charged electrode [13]. The EOF may seem to complicate the device operation. However, we plan to utilize an electrically neutral species as the EOF marker, similar to the capillary electrophoresis devices [21]. If we can simultaneously measure the electrokinetic mobilities of charged and electrically neutral species, we can directly calculate the electrophoretic mobilities of the charged species using Eq. (11).

3.3. The electrokinetic/hydrodynamic focusing process. The working principle of the device is to counter–balance the electrokinetic and pressure–driven flows to form a focusing point for each species. We demonstrate the electrokinetic/ hydrodynamic focusing concept using the geometry shown in Fig. 1. We will first ignore the EOF for simplicity. This can be achieved using either static or dynamic polymer coatings that suppress the electrostatic charges on the wall [22–25]. We will address EOF effects and the experimental procedure separately in Section 3.5. Given the electric field direction in Fig. 1, positively charged particles supplied from a reservoir downstream of the main channel will migrate upstream towards the cathode. Although the electrokinetic velocity of each species is a constant in the entire device, species swimming upstream experience increased PDF in the opposite direction to their motion. This results in reduction of the species net velocity (u_{net}) depending on the local channel averaged velocity of the PDF

$$u_{net} = -u_{epi} + \bar{u_i} \tag{12}$$

Since PDF is stronger in the upstream of the device, under an appropriate flowrate $(\dot{q})$ and electric field (E), we obtain a focusing point, where the species net velocity becomes zero. Using Eqs (8), (10), and (12) this leads to

$$\mu_{ek,i} = \frac{\dot{q}/E}{h_i}. \tag{13}$$

Since $\dot{q}$ and E are fixed, the maximum and minimum electrokinetic mobilities will be observed at the inner and outer channels, respectively. Specifically, using equation (13) we obtain

$$\frac{\mu_{ek,i}}{\mu_{ek,o}} = \frac{h_o}{h_i}. \tag{14}$$

This shows that we can control the device resolution simply by changing the number and position of the splitter channels (h_i). For example choosing $h_o = (1.0 - 0.1 \times i) \times h_i$, we imposed 10% mobility demarcations in each channel. In addition, using 5 channels we obtain a measurement range of $\frac{1}{2}\mu_{ek,o} \leq \mu_{ek} \leq \mu_{ek,o}$. Independent control over the flow rate and the applied electric field enables a wide range of possibilities for the maximum mobility value $\mu_{ek,o}$ in the device, as can be deduced using Eq. (13). In addition, the mobility–range and precision is determined by the device geometry.

Figures 3 and 4 show the snapshots of species migration at different times for $\Delta L = 10h_o$ and $\Delta L = 4h_o$ cases, respectively. Time t is normalized using the convective time scale based on the Helmholtz–Smoluchowski velocity (h_o/u_{HS}), which is the intrinsic velocity scale for electroosmotic flows, and it is given by Eq. (2). Results at $t^* \geq 250$ correspond to the long time behaviour of convective diffusive transport in the device. The focusing point (location where the species/buffer interface crosses the channel center line) is independent of time for $t^* > 200$. The actual time for focusing depends on the device size, species mobility, magnitude of the electric field and the pressure driven flowrate, as will be discussed in the following section.

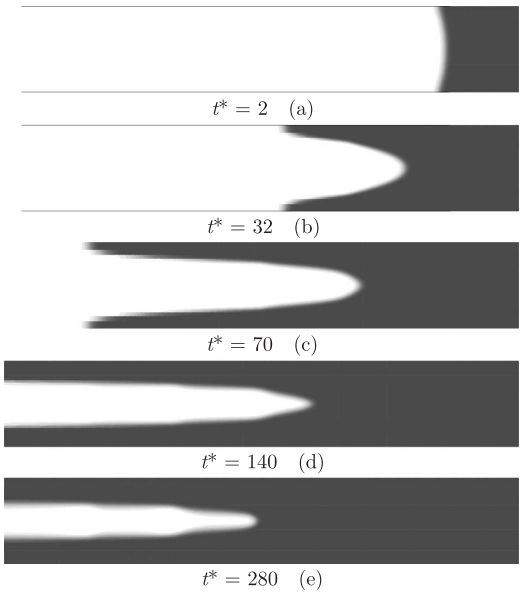

Fig. 3. The contour plots of charged species migration at various times, obtained for the "digitized" version of the device. Steady conditions are observed for $t^* \geq 200$. Since diffusion is unimportant in the device, only two contour colors are used. The cases of $c^* = 0$ and $c^* = 1$ are shown by white and dark contours, respectively

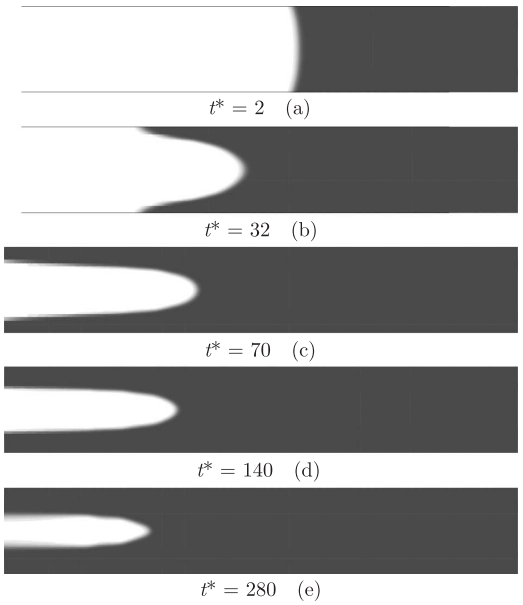

Fig. 4. The contour plots of charged species migration at various times, obtained for the "analog" version of the device. Steady conditions are observed for $t^* \geq 200$

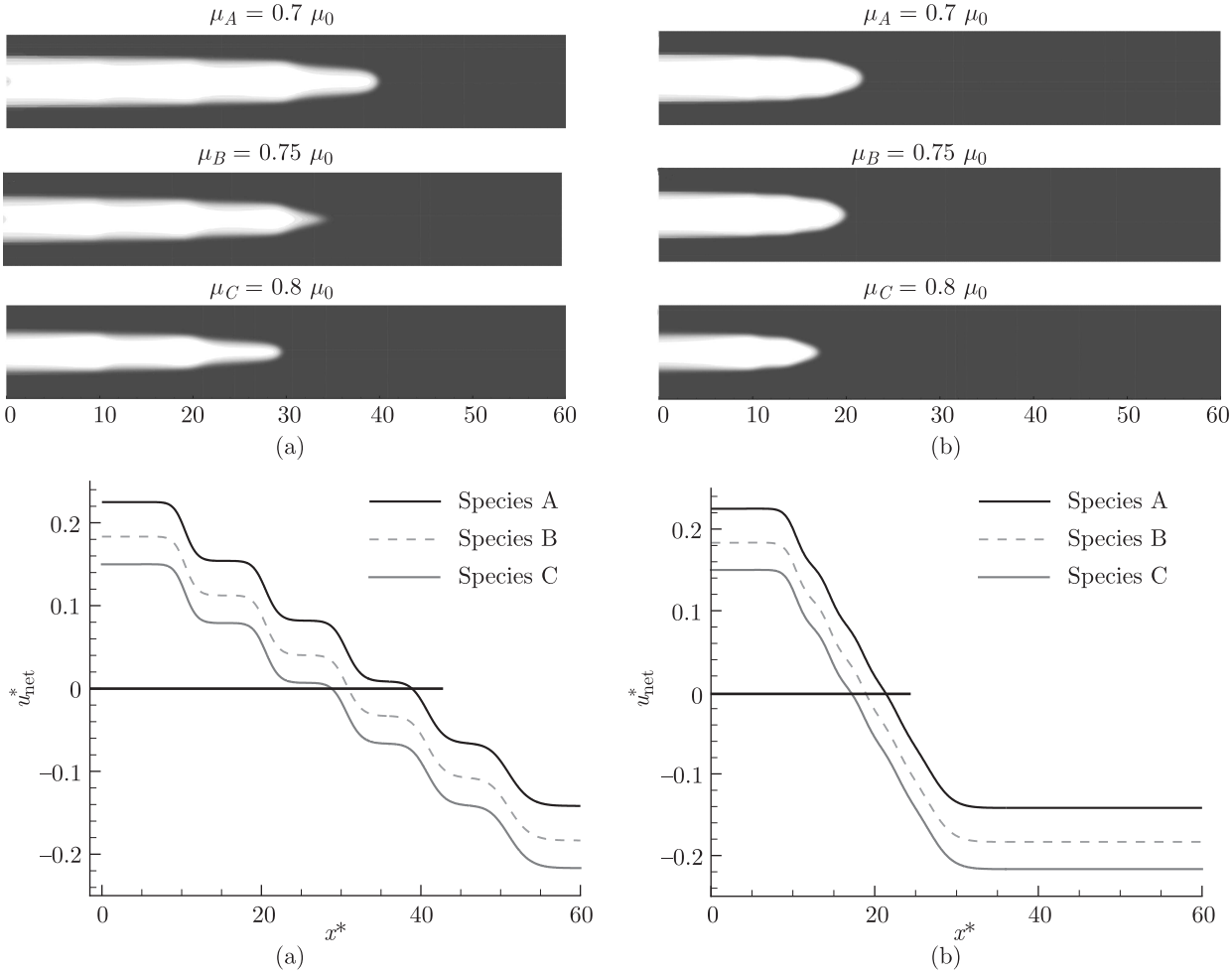

Fig. 5. Focusing point for “digitized” version of the device (a) and “analog” version of the device (b). In both cases, three species with $\mu_A = 0.7\mu_0$, $\mu_A = 0.75\mu_0$, and $\mu_A = 0.8\mu_0$ were tested, where μ_0 is the mobility corresponding to the value that would focus at the inner most channel. The corresponding centerline velocity for the “digitized” (c), and “analog” (d) versions of the device are also shown

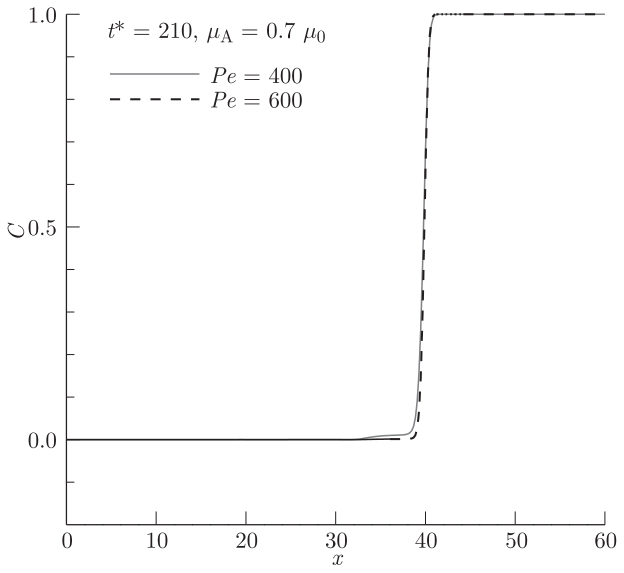

Fig. 6. Comparison of concentration distribution along the centerline of the micro–channel for $Pe = 400$ and $Pe = 600$ under steady state conditions

In Fig. 5 we present the electrokinetic/hydrodynamic focusing in two device configurations. The case with $\Delta L = 10h_o$ is shown on the left column, while the $\Delta L = 4h_o$ case is shown on the right. The species concentration contour plots are obtained for three different electrically charged species with electrokinetic mobilities of $\mu_A = 0.70\ \mu_o$, $\mu_B = 0.75\ \mu_o$, and $\mu_C = 0.80\ \mu_o$, which show distinct focusing points in both devices. Using Eq. (12), we calculated the net species velocity at the centerline of each device. The bottom plots show variation of u^*_{net} as a function of the streamwise location x^*. Despite small changes in the mobility, we observe three distinct focusing locations for three different electrically charged species.

The device with $\Delta L = 10h_o$ gives distinct focusing zones separated from each other. Hence, one can calculate the species mobility within a certain range $\Delta\mu_{ep}$ bounded by the theoretical mobility values at the neighboring channels. We named this the “digitized" version of the device. However, the second configuration ($\Delta L = 4h_o$) results in linear variation in species net velocity at the channel center as a function of x^*. This enables continuous mobility information, and we named this the “analog" version of the device.

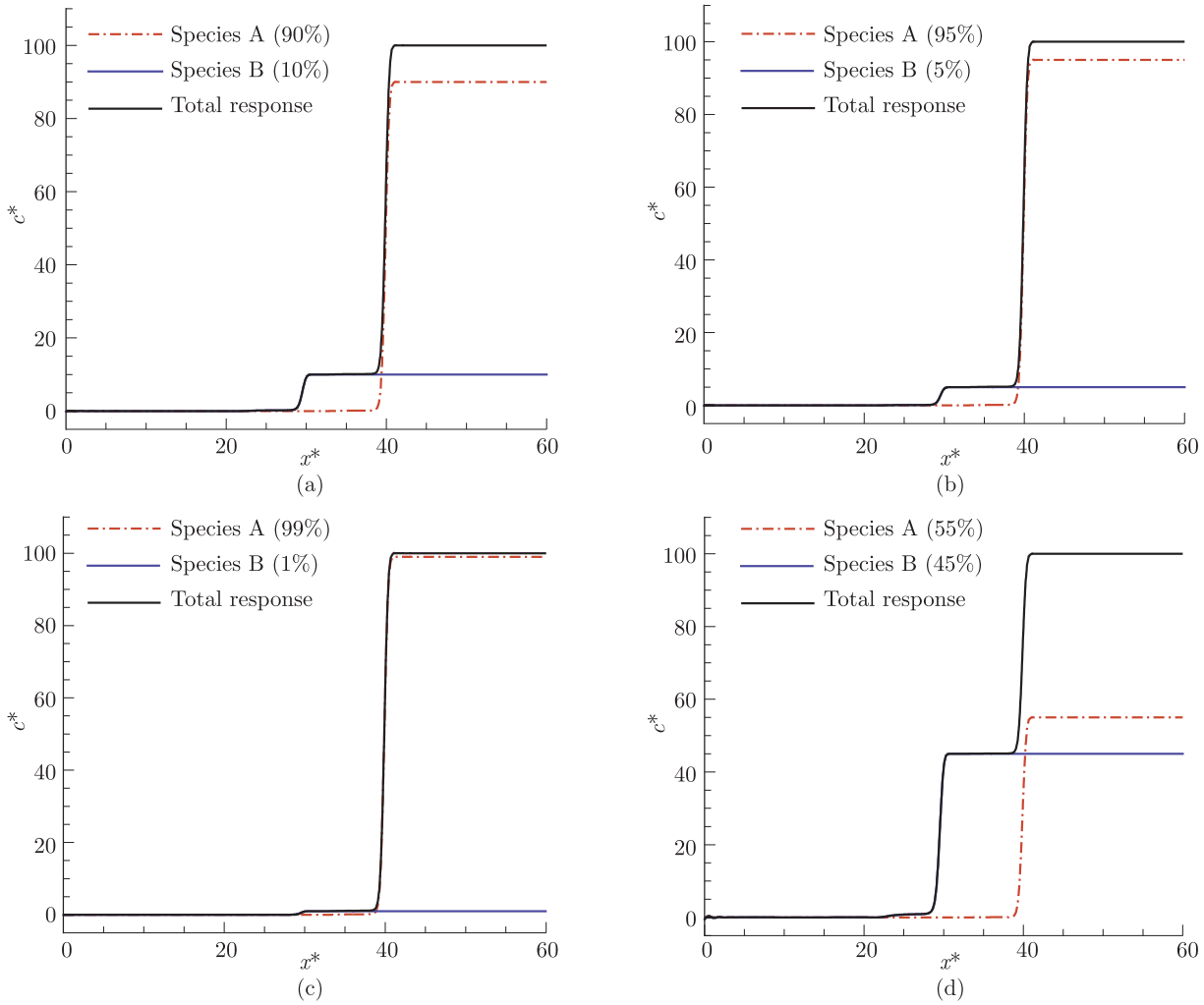

Fig. 7. Multiple species detection along the centerline of the micro-channel using superposition in the "digitized" version of the device. Species transport simulations were conducted at $Re = 0.01$ and $Pe = 1000$

3.4. Experimental procedure and detection. In the following we discuss the basic experimental procedure to be used in the actual prototype device. The direction and magnitude of the electric field and PDF should be chosen as a function of the species charge polarity (positive or negative), which may not be known prior to the measurements. Therefore, experiments can be started by applying an electric field in a preferred direction, and observing whether the mixture enters the micro–device or not. If the mixture (with unknown electrokinetic mobilities) does not enter the device, this may be due to the following two reasons: First, the electroosmotic flow may be stronger and in the opposite direction to the electrophoretic transport. Second, the species may be oppositely charged than what was previously anticipated. These situations can be compensated by reversing the electric field direction or adjusting the pressure driven flowrate, as will be discussed in Section 3.5. For a mixture of positively and negatively charged multiple species, the device will separate the species based on their electrokinetic mobilities. For given PDF and electric field conditions, only the species with either the positive or negative electrokinetic mobilities (μ_{ek}) will be able to enter the device. In fact, this may be very useful for initial screening of the mixture and species sepration. Adjusting the magnitude of the electric field and the flow–rate alter the sensitivity and the range of mobility measurements.

Species diffusion effects. The Reynolds number based on the PDF flow rate and half channel height of the main channel (h_5) is $Re = 0.01$. Despite this low Re, we imposed Peclet number $Pe = 1000$ for our simulations in Figs. 3-5, corresponding to $Sc = 1 \times 10^5$. To investigate the Peclet number dependence of our device, we simulated two additional cases at $Pe = 400$ and $Pe = 600$. In Fig. 6 we plot the concentration variation at the channel center as a function of the streamwise position (x^*) for both simulations, obtained for $t^* > 200$. We observe that diffusion effects are insubstantial at the channel center for $Pe \geq 400$. We must also note that the focusing point is the only location that experiences zero net velocity, and any other location in the domain experiences convective/diffusive transport. We believe that finite convective effects near the focusing point is the reason for limited species diffusion in the device.

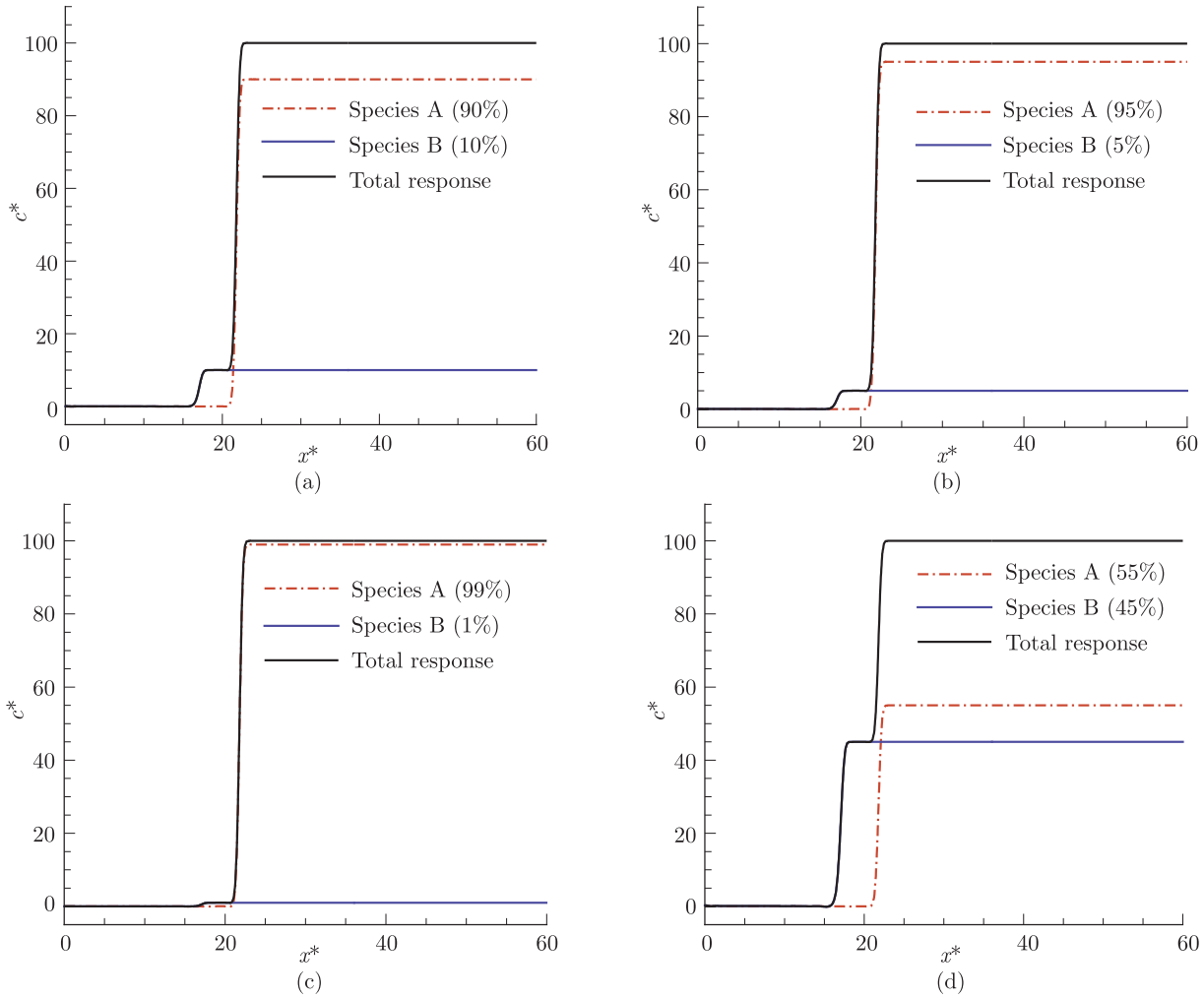

Fig. 8. Multiple species detection along the centerline of the micro-channel using superposition in the "analog" version of the device. Species transport simulations were conducted at $Re = 0.01$ and $Pe = 1000$

Multiple species detection. One of the main features of the device is formation of stationary focusing points after the species migration process reaches to a steady–state. This enables superposition of results obtained separately so that we can measure multiple species mobility for dilute mixtures. Measurement of species concentration along the channel center line using confocal scanning microscopy can yield this information. Knowing the species concentration behavior along the channel center line enables us to determine the number of species and their relative concentration in the mixture. For example, given the concentration variation on the top left plot of Fig. 7, we observe that the mixture has two components with distinct electrokinetic mobilities because we observe two step wise variations in intensity along the channel center. One component has relative concentration of 10% and it is focused at $x^* = 30$. From the focusing point we realize that this component has $\mu_{ek} = 0.8\mu_0$, where μ_0 is the electrokinetic mobility at the inner most channel, and its value can be calculated using Eq. (13). The second component focusing at $x^* = 40$ constitutes 90% of the mixture, and it has a mobility value of $\mu = 0.7\mu_0$. In order to investigate the device resolution we present concentration variation at different relative concentration combinations in Figs 7 and 8. From the results of 90% vs 10%, 95% vs 5%, 99% vs 1%, and 55% vs 45% relative concentration compositions, we realize that the proposed method can identify the composition with as small as 1 % resolution in the "digitized" (Fig. 7) and "analog" (Fig. 8) versions of the device under ideal conditions. However, we must add that the actual experiments may suffer loss of resolution due to fluctuations in fluorescence intensity and bleaching [26]. Therefore, the actual device may not be able to identify the relative concentration of multiple species as accurately as the numerical simulation results. However, the level of accuracy of the prototype needs to be determined experimentally.

3.5. Physical considerations. The proposed device requires large aspect (width to height) ratio channels to minimize the species dispersion due to three-dimensional pressure driven flow. This requires channel widths that are about an order of magnitude larger than the channel heights. Since h_5 is the half channel height, we will select $W = 20h_5$. However, this large aspect ratio geometry may induce problems

in device-fabrication and concentration measurements. Microfabrication of large aspect ratio channels require LIGA or deep reactive ion etching techniques [27]. It is also possible to fabricate a prototype using a micro-CNC. However, the inner channel spacing (h_o) may be too small to use such miniaturized conventional fabrication methods. We envision fluorescence intensity measurements of "fluorescently tagged" species, which requires a species pretreatment process. In addition, fluorescence intensity must be measured sufficiently away from the top and bottom surfaces to avoid strong species dispersion near these surfaces under the effect of pressure driven viscous flow. Such measurements can be achieved using confocal laser scanning microscopy (CLSM), which enables focusing onto a certain channel depth. However, the focal plane must be sufficiently away from the top and bottom surfaces of the device, and preferably near the channel half width ($\simeq W/2$), which is a symmetry axis for the flow and species transport. To minimize the dispersion effects, we have selected $W = 20h_5$. This requirement, along with the maximum depth of the focal plane utilized in the CLSM system being $\simeq 500$ μm, induces limitations on the actual device dimensions. In addition, several measurements need to be taken along the channel axis due to the limited field of view (300 μm$\times$ 300 μm) of the microscope, and the length of the device that is on the order of a few millimeters. Finally, the fluorescence intensity may bleach due to large channel width filled with fluorescently tagged particles, which may have adverse effects on the device sensitivity.

Next we discuss typical device dimensions and the time–scales for hydrodynamic/ electrokinetic focusing process. The CLSM based fluoresce measurements restrict dimensions of the device to $W/2 = 500$ μm, and consequently the large aspect ratio requirement results in $h_5 = 50$ μm. Given that h_5 is the half channel height of the largest microchannel (Fig. 1), we determine $h_o = 25$ μm for $\mu_5 = 0.5\mu_o$ using Eq. (14). Once we select h_o, the minimum physical dimensions of the "digitized" and "analog" versions of the device become $L = 1.5$ mm and $L = 0.6$ mm, respectively. Such device dimensions are typical of microfluidic systems utilized in μ-TAS applications.

For a fixed geometry, the device mobility range is a function of the hydrodynamic flowrate and the axially applied electric field, as determined by Eq. (13). This makes it rather difficult to give specific examples for the device operation conditions. However, we will give a specific example by first analyzing the hydrodynamic/electrokinetic focusing of electrically neutral species in deionized water and a device made out of glass. The ionic concentration of deionized water is 1 μM, and the zeta potential for glass is about $\zeta \simeq -25.4$ mV. Using these values in Eq. (2), we calculate an electroosmotic velocity of $u_{HS} = 0.5$ mm/s at $E = 25$ V/mm (Note that positive value of u_{HS} shows that the EOF is in the electric field direction in Fig. 1). Under these typical conditions, the dimensional time-scales in the device are predicted using $t = t^* h_o/u_{HS}$. Considering that the steady hydrodynamic/electrokinetic focusing was observed in Figs 3 and 4 at $t^* \simeq 200$, these time-scales actually correspond to $t \simeq 10$ s. Therefore, the actual time-scales for the measurement are on the order of tens of seconds, which is an important advantage of the proposed device.

Next we outline a procedure to calculate the electrophoretic mobilities of charged species reported in Fig. 5. Since the glass surface is negatively charged, the electrical double layer is positively charged. Using the electric field direction in Fig. 1, the electroosmotic flow will be towards the cathode. Therefore, the electrically neutral species will migrate upstream (towards left in the figure) and focus near the inner most channel with channel half height of h_o. The electrokinetic mobility of electrically neutral species is equal to their electroosmotic mobility (Eq. 11), and this is given by $\mu_{eo} = u_{HS}/E = 0.02083$ mm^2/Vs. If we consider that electrically neutral species will focus in the smallest channel, only the negatively charged species will be focused in the device, while the positively charged species will move faster, and pass through the inner most channel. If there were any positively charged species in the mixture, we would have detected a uniform fluorescence intensity at the inner most channel, as a result of this situation. Therefore, the focusing results shown in Fig. 5 correspond to electrokinetic mobility measurements of negatively charged species only. Using Eq. (11), we calculate the "electrophoretic mobility" of the species as $\mu_{ep,A} = -0.00625$ mm^2/Vs, $\mu_{ep,B} = -0.00521$ mm^2/Vs, and $\mu_{ep,C} = -0.004166$ mm^2/Vs, where the negative sign indicates polarity of the species charge. Electrophoretic mobility detection of positively charged species require performing the same experiment under increased pressure driven volumetric flowrate so that the electrically neutral species focus in the outer most channel (h_5). This will make the positively charged species focus within the device and enable measurement of their electrophoretic mobilities, provided that the mobility values are within the range of the device, as can be determined using Eq. (13).

4. Conclusions

We presented a device concept for detection of electrophoretic mobility and relative concentration of multiple species based on their electric charges. The proposed method have the following features:

1. The hydrodynamic/electrokinetic focusing point is independent of time and it solely depends on the electrokinetic mobility of the species for fixed geometry, PDF and axial electric fields.

2. Despite the low Reynolds number flow, results at the focusing point show minimal diffusion effects for species with high Schmidt numbers.

3. Knowing the pressure driven flow rate and the applied electric field, one can easily utilize the device to measure a wide range of electrokinetic mobilities.

4. The proposed method utilizes constant sample feeding, and hence the results are independent of the initial sample distribution.

5. The time-scales for measurement are on the order of tens of seconds, which is an important aspect of the proposed device, especially for μ-TAS applications.

Although the first two features would also be observed in the isoelectric focusing technique, the IEF maintains such conditions under axial pH gradients, which are rather difficult to maintain in microchannels [10]. The proposed method is advantageous over capillary electrophoresis, which results in time-dependent measurements with substantial Taylor dispersion effects. In addition, the CEP requires a well defined initial sample distribution for better detection accuracy. However, such shortcomings are avoided in the proposed device. Regardless of the physical difficulties discussed in Section 3.5, the proposed device can be utilized for quick screening (within an order of tens of seconds) of biologicals and chemicals based on their electrical charge and electrokinetic mobilities, enabling identification of the constituents of dilute mixtures. Further developments of this concept requires three-dimensional simulations and experiments on a prototype device.

Acknowledgements. Partial funding for this research was provided by the National Science Foundation under Grant No. 0306622.

References

[1] R.F. Probstein, *Physicochemical Hydrodynamics*, Wiley and Sons Inc.,1997.

[2] M. Melvin, *Electrophoresis*, John Wiley and Sons Inc, London, 1987.

[3] W.L. Tseng and H.T. Chang, "A new stategy for optimizing sensitivity, speed, and resolution in capillary electrophoretic separation of DNA", *Electrophoresis* 22, 763–770 (2001).

[4] K. Kleparnik, Z. Mala, and P. Bocek, "Fast separation of DNA sequencing fragments in highly alkaline solutions of linear polyacrylamide using electrophoresis in bare silica capillaries", *Electrophoresis* 22, 783–788 (2001).

[5] M. Saur, B. Angerer, W. Ankenbauer, Z. Foldes-Papp, F. Gobel, K.T. Han, R. Rigler, A. Schulz, J. Wolfrum, and C. Zander, "Single molecule DNA sequencing in submicrometer channels: state of the art and future prospects", *Journal of Biotechnology* 86(3), 181–201 (2001).

[6] P.G. Righetti, *Isoelectric Focussing: Theory, Methodology and Applications*, Elsevier Biomedical, Amsterdam, 1983.

[7] K. Macounova, C.R. Cabrera, M.R. Holl, and P. Yager, "Generation of natural pH gradients in microfluidic channels for use in soelectric focusing", *Anal. Chem.* 72 (16), 3745–3751 (2000).

[8] K. Macounova, C.R. Cabrera, and P. Yager, "Concentration and separation of proteins in microfluidic channels on the basis of transverse IEF", *Anal. Chem.* 73 (7), 1627–1633 (2001).

[9] C.R. Cabrera, B. Finlayson, and P. Yager, "Formation of natural pH gradients in a microfluidic device under flow conditions: model and experimental validation", *Anal. Chem.* 73 (3), 658–666 (2001).

[10] C.H. Horiuchi, P. Dutta and C.F. Ivory, "Isoelectric focusing in a poly(dimethylsiloxane) microfluidic chip", *Analytical Chemistry* 77 (5), 1303–1309 (2005).

[11] R. Westermeier, *Electrophoresis in Practice*, VCH Publishers Inc, New York, 1990.

[12] P. Janos, "Role of chemical equilibria in the capillary electrophoresis of inorganic substances", *Journal of Chromatography* A 834, 3–20 (1999).

[13] G.E. Karniadakis, A. Beskok, and N. Aluru, *Microflows and Nanoflows: Fundamentals and Simulation*, Springer-Verlag, New York, 2005.

[14] P. Dutta and A. Beskok, "Analytical solution of time periodic electroosmotic flows: analogies to Stokes' second problem", *Anal. Chem.* 73, 5097–5102 (2001).

[15] X. Niu, and Y.K. Lee, "Efficient spatial-temporal chaotic mixing in microchannels", *J. Micromech. Microeng.* 13, 454–462 (2003).

[16] A. Beskok and T.C. Warburton, "Unstructured hp finite-element scheme for fluid flow and heat transfer in moving domains", *Journal of Computational Physics* 174, 492–509, (2001).

[17] G.E. Karniadakis and S.J. Sherwin, *Spectral/HP Element Methods for CFD*, Oxford University Press, Oxford, 1999.

[18] G.E. Karniadakis, M. Israeli, and S.A. Orszag, "High-order splitting methods for the incompressible Navier-Stokes equations", *Journal of Computational Physics* 97, 414–443 (1991).

[19] P. Dutta, A. Beskok, and T. Warburton, "Electroosmotic flow control in complex microgeometries", *J. Microelectromechanical Systems* 11 (1), 36–44 (2002).

[20] M.J. Kim, A. Beskok, and K.D. Kihm, "Electro-osmosis-driven micro-channel flows: a comparative study of microscopic particle image velocimetry measurements and numerical simulations", *Experiments in Fluids* 33, 170–180 (2002).

[21] E.V. Dose and G. Guiochon, "Time scales of transient processes in capillary electrophoresis", *Journal of Chromatography* 652, 263–275 (1993).

[22] D. Kaniansky, M. Masar, and J. Bielcikova, "Electroosmotic flow separation for capillary zone electrophoresis in a hydrodynamically closed separation system", *J. Chromatogr.* A 792, 483–494 (1997).

[23] Y. Liu, J.C. Fanguy, J.M. Bledsoe, and C.S. Henry, "Dynamic coating using polyelectrolyte multilayers for chemical control of electroosmotic flow in capillary electrophoresis microchips", *Analytical Chemistry* 72 (24), 5939–5944 (2000).

[24] J. Horvath and V. Dolnik, "Polymer wall coatings for capillary electrophoresis", *Electrophoresis* 22, 644–655 (2001).

[25] P. Righetti, C. Gelfi, B. Verzola, and L. Castelletti, "The state of art of dynamic coatings", *Electrophoresis* 22, 603–611 (2001).

[26] M.A. Holden, S. Kumar, E. Castellana, A. Beskok, and P.S. Cremer, "Generating fixed concentration arrays in a microfluidic device", *Sensors and Actuators* B 92, 1999–2007 (2003).

[27] W. Trimmer, *Micromechanics and MEMS, Classic and Seminal Papers to 1990*, IEEE Press, New York, 1997.